Wheel – Rail Interaction Based on Roughness Calculation

M. VISCARDI, P. NAPOLITANO
Department of Industrial Engineering
University of Naples Federico II
Via Claudio, 80, 80034 Naples
ITALY
massimo.viscardi@unina.it

Abstract: - Rolling noise is a relevant source in railway applications. The rolling noise is generated by the contact force the wheel, and the rail, exchange each other during relative motion. The interaction force between wheel and rail is generated by their roughness. Wheel and rail surfaces are not perfectly flat, they have a lot of small micro imperfections due to usage, damages, manufacturing. The whole of these imperfection is the roughness of the two surfaces. In the following a new interaction model will be shown where the roughness in kept in account to simulate the real case application. The model, based on previously studies, is improved introducing the rail and wheel real roughness for interaction force calculation. A real case study will be kept in account for model application and its application.

Key-Words: - wheel-rail interaction, contact force, roughness, rolling noise, numerical model, railway noise, interaction force.

1 Introduction

The rolling noise is one of the most relevant source in railway application. With engine noise and aerodynamic noise is one of the source contribute to overall noise both for inner noise and pass-by noise. Every source in railway application is relevant in a specific speed range according to Figure 1. For the specific case of rolling noise, it is relevant in range between 40 km/h and 200 kh/h that is a really huge range if compared with engine (0 – 40 km/h) and aerodynamic noise (over 200 km/h), This make the rolling noise the most important source to study and is relevant source for a wide range of trains, from cargo to subway.

The rolling noise is generated by the force wheel and rail exchange each other during the relative motion. The force the two elements exchange is called contact force or interaction force. This force is maiden of two components; the first is the static component due to train weight and is always present; the second contribution comes from dynamic component that depends from train weight and suspension stiffness, the speed of the train, the roughness of wheel and rail. This second contribute will be studied in the following of this work.

The dynamic component of contact force, as said before, depends, among others, by the roughness. We can figure out wheel and rail have a non-perfectly flat surface; the surface of both is full of micro imperfection and these imperfections are the roughness of the two elements. The roughness is due to several factors, the most relevant are usage and damages. Also, when they are completely new the surface is not perfect due to manufacturing process and limitations. In this scenario is relevant to know the roughness and its effect on contact force.

If the roughness is too much the wheel and the rail can be rebored to reduce the roughness overall level. Roughness can be measured with appropriate experimental tests or with methods based on accelerometric measures.

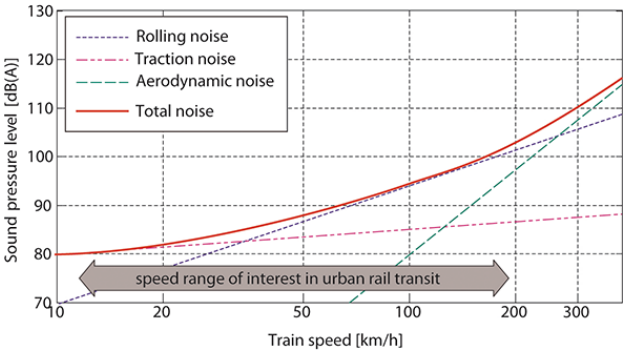

Figure 1: Noise sources in railway.

In a lot of real application wheel roughness is small if compared with rail roughness; this is true for the reason the wheel is rebored often and its roughness is under control. For the rail, the

maintenance operations are distant in time and the usage is greater than wheel usage.

This hypothesis is relevant for model implementation in order to simplify mathematical approach but is not relevant at all and it will be removed in the end of this work.

2 Theoretical Background

We can schematize the train as a concentrated mass (m_w in Figure 2); the concentrated mass is moving with a certain speed $v(t)$, time dependent, along a path $z(t)$. The connection between the mass and the path is ensured by the linear spring k_H. The vertical displacement induced on the mass by the path is indicated by the function of time $u(t)$.

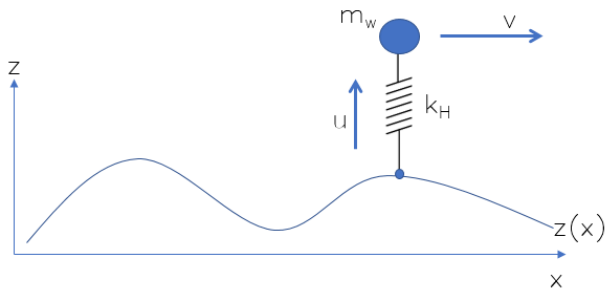

Figure 2: Wheel – rail interaction model schematization.

The wheel – rail interaction problem can be treated as a problem of one object, the wheel, rolling on another object, the rail. Now we can introduce some assumption for simplify the model. The wheel has no roughness and can be considered perfect. The rail can be considered almost perfect with only one imperfection. This imperfection is schematized with a step function.

In general the wheel and rail have only one contact point.

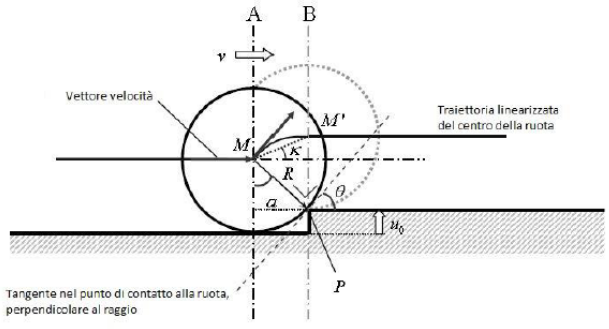

Figure 3: Step input for contact force.

When the rail is in position A (see Figure 3) there are two contact points. Physically the vector indicating the speed has a discontinuity and this is due to a discontinuity change in contact point. From a mathematical point of view the first derivative of displacement is discontinue in position A. The contact force between wheel and rail cannot be calculated in position A as directly consequence of discontinuity in step function derivative in this position.

The simplified model of Figure 3 can be used to calculate the wheel center displacement respect to the time. In this case the displacement, expressed as $z(t)$, can be expressed as

$$z(t) = \frac{u_0}{t_b} tH(t_b - t) + u_0 H(t - t_b) \quad (1)$$

where t_b is the time the wheel needs to move from position A to position B.

2.1 Ramp Input Model

A more complicate case to analyze is the one shown in Figure 4.

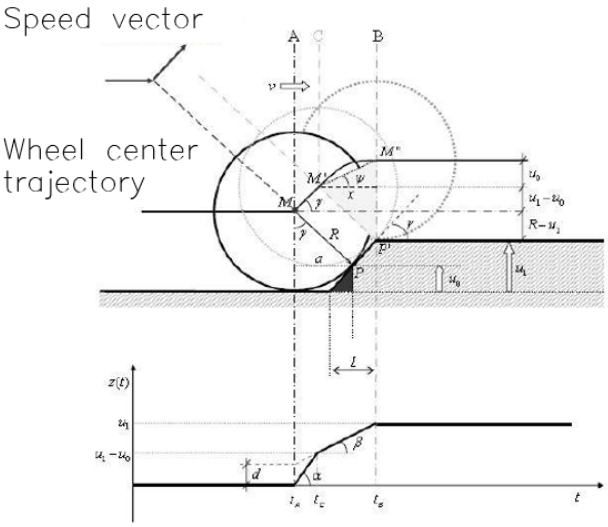

Figure 4: Ramp roughness model.

In this model the step profile is substituted by a double ramp profile. This model is closer to real case and avoid the infinity occurring in step profile. In this case the wheel passing from position A to position B moves through an intermediate position C (see Figure 4). The ramp profile is defined by four parameters, α, β, u_0 and u_1 that represent the angles of the ramps and their height respectively.

In this case the vertical displacement of the wheel center is expressed by a more complicated equation that is expressed in the following.

$$z(t) = \alpha t H(t_{AC} - t) + (\beta t + d)[H(t - t_{AC}) - H(t - t_{BC})] + u_1 H(t - t_{BC}) \quad (2)$$

In the previously equation we have

$$t_{AC} = \frac{2}{\sin(2\gamma)} \frac{u_1 - u_0}{v} \quad (3)$$

$$t_{BC} = \frac{2Ru_0}{vx} \quad (4)$$

The time the wheel needs to move from position A to position C and time the wheel needs to move from position B to position C respectively.

The parameters α and β are defined as follow

$$\alpha = \frac{1}{2}\sin(2\gamma)\, v \quad (5)$$

$$\beta = \sqrt{\frac{u_0}{2R}}\, v \quad (6)$$

And the expression for d is

$$d = (u_1 - u_0)\left(1 - \frac{1}{\sin(2\gamma)}\sqrt{\frac{2u_0}{R}}\right) \quad (7)$$

Substituting equations (3), (4), (5), (6) and (7) into the (2) we can obtain a new expression for wheel center displacement in case of ramp input.

$$z(t) = \gamma v t H(t_{CB} - t) + \left(\sqrt{\frac{u_0}{2R}}\, vt + d\right)[H(t - t_{BC}) - H(t - t_{AC})] + u_1 H(t - t_{BC}) \quad (8)$$

2.1 Ramp Input Model

For a real case consideration we can substitute the custom path $z(t)$ with a real rail. The rail can be considered as beam simply supported at both ends and described by material (Young's modulus, density, Poisson's modulus) and geometry (inertia, frontal area). The rail is also supported by springs.

The moving train is replaced by a fixed mass connected to the rail through a linear spring and can be considered as an harmonic oscillator. (see Figure 5).

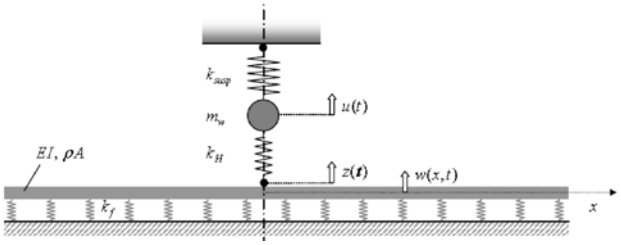

Figure 5: Wheel – Rail interaction model.

The train is subject to a moving force in time domain that can be schematized as a train of impulses in frequency domain according to reciprocity principle.

The system exposed is governed by three following equations; the Eulero-Bernulli equation for beams, the harmonic oscillator equation, the contact force calculated according to Hook law. The three equations are reported below.

$$EI\frac{\partial^4 w(x,t)}{\partial x^4} + \rho A\frac{\partial^2 w(x,t)}{\partial t^2} + k_f w(x,t) = -F(t)\delta(x) \quad (9.a)$$

$$m_w \frac{d^2 u}{dt^2} + k_s u(t) = F(t) \quad (9.b)$$

$$F(t) = k_H[-u(t) + w(0,t) + z(t)] \quad (9.c)$$

The set of equations (9) is a partial differential system; to solve it we need an appropriate set of boundary conditions; the boundary conditions imposed are: 1) no perturbation present far away from the system; 2) the initial position and initial speed are known and constant.

According to these hypotheses the system can be transformed from time domain to Laplace domain.

Into the Laplace domain the set of equations can be expressed as

$$\tilde{w}(x,s) = -\frac{\tilde{F}(s)}{16EIk_0}\left[(1-i)e^{-(1+i)k_0|x|} + (1+i)e^{(-1-i)k_0|x|}\right] \quad (10.a)$$

$$-m_w\dot{u}(0) + (m_w s^2 + k_s)\tilde{u}(s) = \tilde{F}(s) \quad (10.b)$$

$$\tilde{F}(s) = k_H[-\tilde{u}(s) + \tilde{w}(s) + \tilde{z}(s)] \quad (10.c)$$

From system (10) we can solve for the force and the wheel center displacement to obtain the contact force between wheel and rail.

The following equations are shown in the following.

$$\tilde{F}(s) = \frac{\tilde{z}(s) - \frac{m_w v_0}{m_w s^2 + k_s}}{\frac{1}{k_h} + \frac{1}{m_w s^2 + k_s} + \frac{1}{8EIk_0^3}} \quad (11)$$

$$\tilde{z}(s) = \sqrt{\frac{u_0}{2R}}\frac{v}{s}\left(1 - e^{-\sqrt{2Ru_0}\frac{s}{v}}\right) \quad (12)$$

Equations (11) and (12) solve the contact force problem in Laplace domain but they give no information about what happens in time domain.

To convert the result from Laplace domain to time one we can use the following

$$F(t) = \frac{e^{\sigma t}}{2\pi}\int_0^{+\infty} Re\left(\tilde{F}(s)\right)e^{i\omega t}\,d\omega \quad (13)$$

3 Rail Roughness

The real surface of rail and wheel is full of micro imperfections due to several factors. The most relevant factor is the usage of the two elements. For the wheel the roughness problem is, usually, not so relevant due to the frequent maintenance it has during lifecycle. For the rail this is not true; the rail has a lifecycle longer than the wheel and less maintenance.

In Figure 6 is shown a classical example of roughness for a rail.

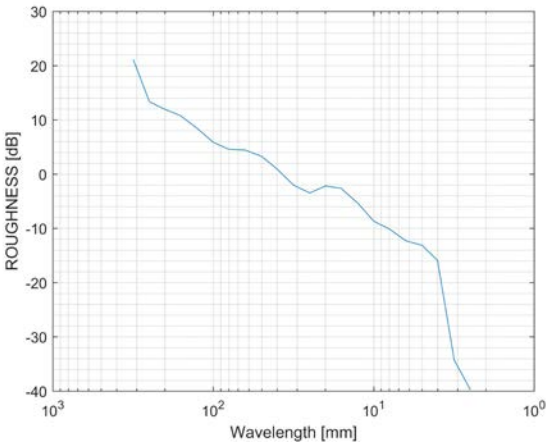

Figure 6: Rail roughness measured.

The roughness can be calculated with an experimental setup. Usually the roughness is calculated along the rail and the roughness of wheel is not kept in account.

The proposed method for roughness calculation involve an alternative approach measuring the acceleration during a train pass-by. The advantage of this method is the capability to calculate the equivalent roughness of wheel and rail combined.

3.1 Acceleration Measurements

As said before, for roughness calculation, the acceleration on the rail is measured among during pass-by of the train at constant speed.

The acceleration was measured during multiple train pass-by to obtain a mean value of acceleration.

For accelerometer measurements a set of accelerometers was used. According to reference norm they were place on the railway is appropriate positions. As shown in Figure 7 the accelerometer position is defined by norm and have been repeated on experimental test as shown in Figure 8. Acceleration spectra along the z axis will be the basic input for the track decay calculation [6-7]; with acceleration along y, with a similar process, the longitudinal decay rate may be calculated. Because this parameter is less useful , it will be not presented within this paper.

In this specific test, three tri-axial accelerometers have been used also to avoid problem related to the need of compensating profiles. Also, an extra accelerometer has been positioned on the rail web for further consideration; it has not been used for the purposes of the work.

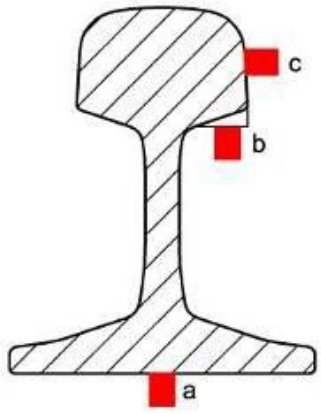

Figure 7: Acceleration measurement point on the rail.

Above is shown the acceleration has been measured for all accelerometers for more than one passage. An acceleration example in shown in Figure 9 where a typical passage is plotted as function of time. For decay rate calculation only vertical acceleration will be considered and only decay rate used for roughness calculation.

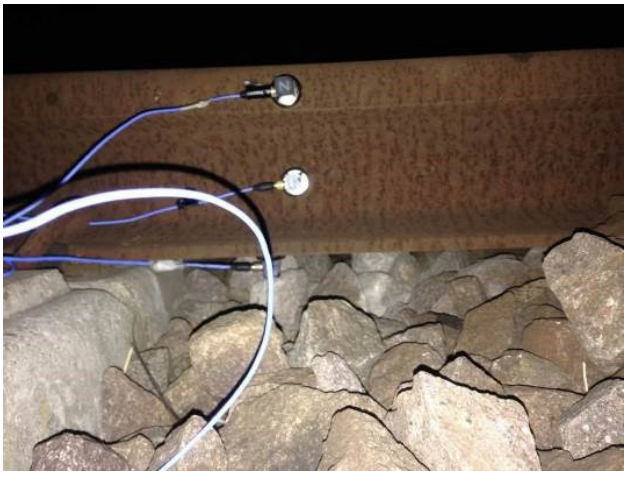

Figure 8: Real accelerometers installation.

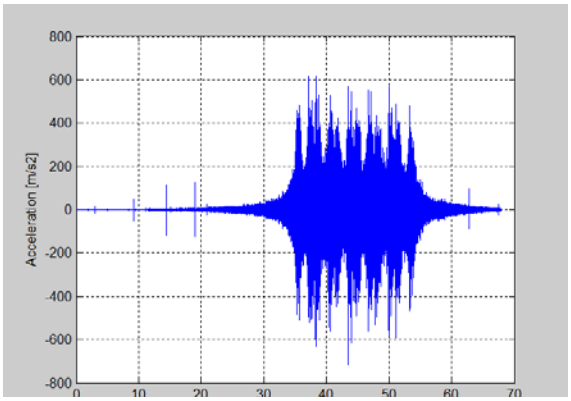

Figure 9: Acceleration time history pass-by noise.

3.2 Roughness Calculation

Once that acceleration has been measured, according to normative the first step for roughness calculation is the decay rate calculation that depends from the FRF of the system. The FRF has been calculate on whole train passage and around a single wheel passage. The difference between two are shown in figure 10 and 11.

Using the iterative method and a residual error of 10- 5 the decay rate is than calculate for a wide number of measures as shown in Figure 12. The mean value of decay rate is than used for roughness calculation.

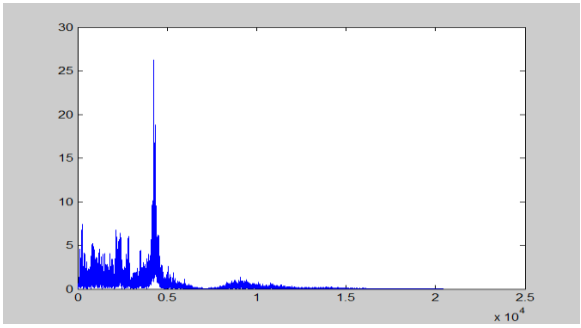

Figure 10: FRF measured on whole passage.

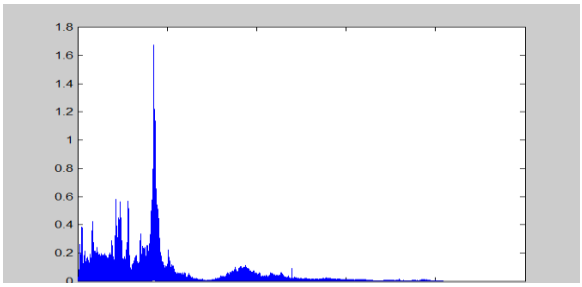

Figure 11: FRF for single wheel passage.

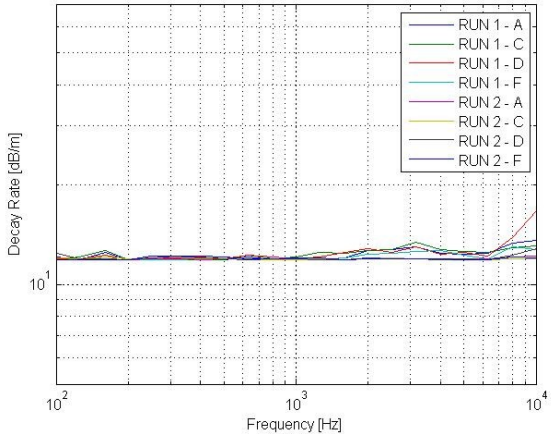

Figure 12: Multiple pass-by decay rate.

4 Interaction Force Model

The roughness calculated in previously chapter can now be used to update the contact model. In chapter 2 we have introduced the contact force calculation in the ideal hypothesis of an impulse sequence.

In real case application the roughness, as shown, is not easy to schematize as a train of impulse and must be rearranged to be used inside the model.

From previously chapter we know the roughness is given in wavelength domain but it is not useful for real case application. The first step is transform wavelength domain to time domain and we can do it passing through frequency domain.

The frequency domain and the wavelength domain are related thorough the speed of train according to following equation

$$f = \frac{v}{\lambda} \tag{14}$$

where f is the frequency and λ is the wavelength. The speed of train is a relevant parameter and its change cause a shift of the roughness along the frequency domain.

Knowing the curve in frequency domain we can extrapolate the time shape of the rail profile. We can suppose the rail roughness is periodic along each piece of rail and repeats itself in time. In this case the time profile can be calculated according to the Fourier approach.

According to Fourier the time profile can be represented according the sum of an infinite number of sinus functions. In this case the members of Fourier series is finite and the profile can be written as

$$u(t) = u_0 + \sum_{i=1}^{N} A_i \sin(2\pi f_i t) \tag{15}$$

The given profile depends from the speed as primary parameter.

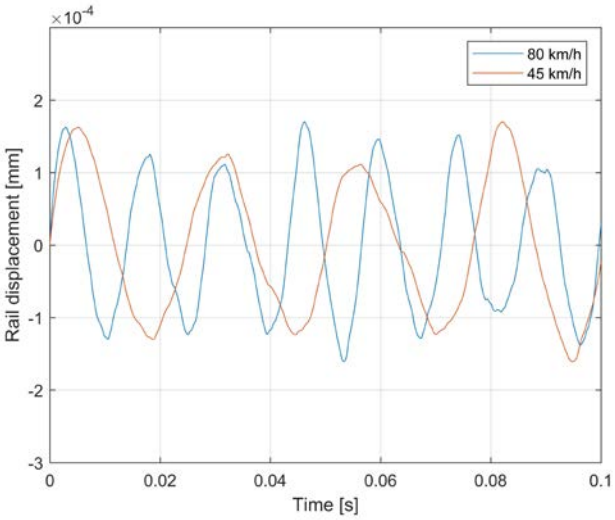

Figure 13: Roughness profile calculated for different speeds.

In Figure 13 is shown the rail profile calculated for two different speeds (45 km/h and 80 km/h).

Looking at Figure 13 we can print out some conclusions about the roughness shape versus time. We can notice the amplitude of the roughness is not dependent from the speed. The roughness amplitude, in fact, is a rail property and not depends from the speed at all. Increasing the speed, the peaks become closer and closer; closer peaks mean a higher frequency excited.

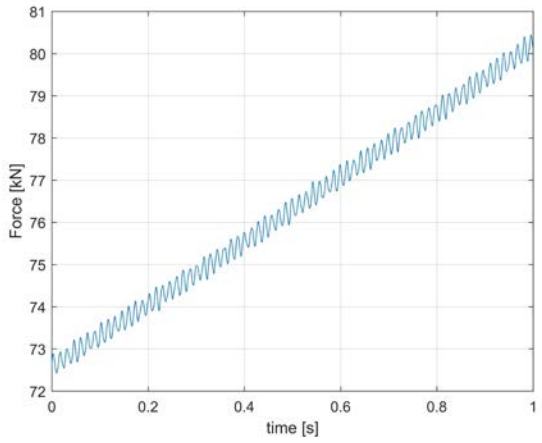

Figure 14: Contact force in time domain.

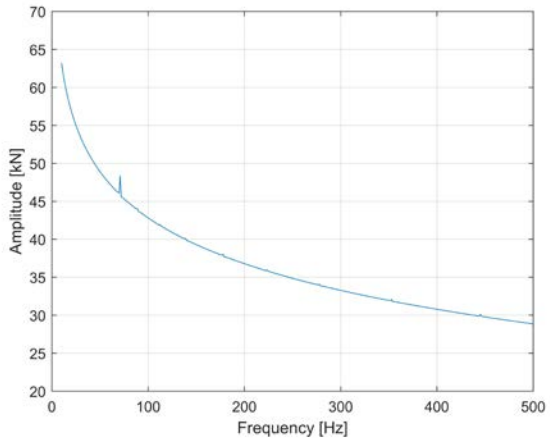

Figure 15: FFT of contact force.

4.1 Time Dependent Model

Knowing the rail profile in time domain we can come back to (11) and (12) to introduce time dependence in them.

We can now suppose to resolve the force and wheel center equations in time step-by-step. We can figure out to divide the simulation time into a finite number of steps as small as necessary. The time step used is relevant for the transformation in frequency domain. In this simulation the time step choose is 0.0001s, this allow us to have the FFT up to 10kHz that is enough for our purpose.

For each step of the simulation we know the rail displacement given by $u(t)$ in equation (15). Using the appropriate value of $u(t)$ is used in (11) and (12) for force calculation.

According to this approach the (11) and (12) are transformed as follow

$$\tilde{F}(s,t) = \frac{\tilde{z}(s,t) - \frac{m_w v(t)}{m_w s^2 + k_s}}{\frac{1}{k_h} + \frac{1}{m_w s^2 + k_s} + \frac{1}{8EIk_0^3}} \quad (16)$$

$$\tilde{z}(s,t) = \sqrt{\frac{u(t)}{2R}} \frac{v(t)}{s} \left(1 - e^{-\sqrt{2Ru(t)}\frac{s}{v(t)}}\right) \quad (17)$$

In this case the model is solved for each time and, instead of one force function, we have a matrix of force functions, one curve for each time.

Having one curve for each time we can apply at each function the equation (13) to transform it back to time domain. As result of this operation we obtain a force value for each time step in which the simulation was split. Coupling together all the time steps we obtain a curve vs. the time that represent the contact force between wheel and rail in time domain.

In Figure 14 is shown the force vs time for a real test case. The force shape is defined by two different components; the static force that give the carrier wave and the dynamic component. The growing shape is due to the presence of the static force at 0Hz.

In Figure 15 is show the FFT of the time dependent curve of contact force. The highest contribute of force is in the range between 0 – 500 Hz with a peak related to the speed of the train.

5 Conclusions

The model shown is an advance in contact force interaction model. The mathematical model, based on a sequence of impulses, is extended to keep in account the real roughness of the rail.

The roughness used in the model, if calculated with proposed method, is a combined roughness of wheel and rail. If we use a combined roughness we have a real case application and the results is related to a specific combination of train and wheel.

By the way the model is completely generic and is independent from the roughness used as input. Changing the roughness and the calculation method the method is still valid and results still reliable.

The method to divide the wheel and rail roughness is to use the proposed method with a new wheel having a roughness neglectable respect the rail one. In this case the roughness can be ascribed to the rail only. The roughness of the wheel can after added to the rail roughness for the entire simulation purpose.

References

1. Thompson, D.J., Wheel-Rail Noise Generation, Part I: Introduction and Interaction Model, Journal of Sound and Vibration,161, 1993a.

2. Thompson, D.J., Wheel-Rail Noise Generation, Part II: Wheel Vibration, Journal of Sound and Vibration,161, 1993b.

3. Thompson, D.J., Wheel-Rail Noise Generation, Part I: Inclusion of wheel rotation, Journal of Sound and Vibration,161, 1993c.

4. Thompson, D.J., Experimental Analysis of Wave Propagation in Railway Propagation in Railway Track, Journal of Sound and Vibration, 203(5), 1997.

5. James T. Nelson, Transit Cooperative Research Program - Wheel/Rail Noise Control Manual TCRP report 23.

6. Ente Italiano di Normazione, UNI/CT 050 , FprCEN/TR 16891 "Railway applications - Acoustics - Measurement method for combined roughness, track decay rates and transfer functions".

7. Massimo Viscardi, Pasquale Napolitano, Stefano Ferraiuolo, An Innovative Procedure for the Rolling Noise Evaluation, Doi. 10.1051/matecconf/20167605013

8. Massimo Viscardi, Pasquale Napolitano, Maurizio Arena, AN INNOVATIVE NUMERICAL APPROACH FOR RAILWAY ROLLING NOISE FORECAST, MATEC , (2017) Proceedings of the ICSV24 (24th International Conference of Sound and Vibrations)

9. Siano D., Viscardi M., Panza, M.A., Acoustic Optimization of a High-speed Train Composite Sandwich Panel Based on Analytical and Experimental Transmission Loss Evaluation Integrated by FE/Test Correlation Analysis Energy Procedia 81:689-703 · December 2015 DOI: 10.1016/j.egypro.2015.12.075

10. Massimo Viscardia ,Pasquale Napolitano, Stefano Ferraiuolo, Experimental Validation Of An Innovative Procedure For The Rolling Noise Correction (2017) Proceedings of the CSCC17 Conference, MATEC Web of Conferences (2017)

11. G. Iannone, C. Guarnaccia, J. Quartieri, Speed Distribution Influence in Road Traffic Noise Prediction, Environmental Engineering and Management Journal Vol. 12(3), pp. 493-501 (2013)

12. C. Guarnaccia, J. Quartieri, J.M. Barrios, E.R. Rodrigues, Modelling Environmental Noise Exceedances Using non-Homogenous Poisson Processes, Journal of the Acoustical Society of America Vol. 136, (2014) pp. 1631-1639; http://dx.doi.org/10.1121/1.4895662.

13. Magliacano, D., Viscardi, M., Ciminello, M., Dimino, I., Concilio, A. Feasibility study for a tonal vibration control system of a mounting bracket for automotive gearboxes (2016) International Journal of Mechanics, 10, pp. 403-410.

14. Viscardi, M., Rusciano, N., Iadevaia, M., Siano, D. An optimization process experience for HVAC noise emission and flows distribution inside a passenger's train wagon (2009) 16th International Congress on Sound and Vibration 2009, ICSV 2009, 6, pp. 3334-3341.

15. Quartieri, J and Mastorakis, NE and Iannone, G and Guarnaccia, C and D'ambrosio, S and Troisi, A and Lenza, TLL (2009) Recent Advances in Applied and Theoretical Mechanics, 5th SEAS International Conference on Applied and Theoretical Mechanics (MECHANICS'09) Puerto De La Cruz, Tenerife, Canary Islands, Spain December pp 72-80

16. Quartieri, J and Mastorakis, NE and Guarnaccia, C and Troisi, A and D'Ambrosio, S and Iannone, G Traffic noise impact in road intersections (2010) International Journal of Energy and Environment pp 1-8 Issue 1, Volume 4,

17. Viscardi, M., Leo, R.D. Implementation of an Electronic Circuit for SSSA Control Approach of a Plate Type Element and Experimental Match with a Feed-Forward Approach (2016) Archive of Mechanical Engineering, 63 (4), pp. 665-677. DOI: 10.1515/meceng-2016-0038

18. Guarnaccia, Claudio and Mastorakis, Nikos E and Quartieri, Joseph Wind turbine noise: Theoretical and experimental study International Journal of Mechanics pp 129-137 Issue 3, Volume 5, 2011

19. Quartieri, Joseph and Mastorakis, Nikos E and Iannone, Gerardo and Guarnaccia, Claudio A cellular automata model for fire spreading prediction (2010) Latest Trends on Urban Planning and Transportation pp 173-179

20. Quartieri, J and Mastorakis, NE and Guarnaccia, C and Troisi, A and D'Ambrosio, S and Iannone, G Road Intersections Noise Impact on Urban Environment Quality (2009) Proceedings of the 5th WSEAS International Conference on "Applied and Theoretical Mechanics" pp.162-171

21. Viscardi, M., Napolitano, P., Arena, M. Simulation and experimental validation of fatigue endurance limit of copper alloy for industrial applications (2016) International Journal of Mathematical Models and Methods in Applied Sciences, 10, pp. 340-346.